Journal of Photochemistry and Photobiology 3–4 (2020) 100007

Contents lists available at ScienceDirect

Journal of Photochemistry and Photobiology

journal homepage: www.elsevier.com/locate/jpap

A rapid assessment of the radiative properties from a suspension of *Chromochloris zofingiensis*

Manuel Vicente Ibañez[a,b,d,*], Rodrigo Jorge Leonardi[b,c,d], Josué Miguel Heinrich[b,c,d], Juliane Steingroewer[a], Thomas Walther[a], Krujatz Felix[a]

[a] Institute of Natural Materials Technology, TU Dresden, Bergstraße 120, 01069 Dresden, Germany
[b] Instituto de Desarrollo Tecnológico para la Industria Química (INTEC), Consejo Nacional de Investigaciones Científicas y Técnicas (CONICET), Universidad Nacional del Litoral (UNL), Güemes 3450 (S3000GLN), Santa Fe, Argentina
[c] Facultad de Bioquímica y Ciencias Biológicas (FBCB), Universidad Nacional del Litoral (UNL), Ciudad Universitaria (Paraje El Pozo), Santa Fe, Argentina
[d] Grupo de Innovación en Ingeniería de Bioprocesos, Ciudad Universitaria (Paraje El Pozo), Santa Fe, Argentina

ARTICLE INFO

Keywords:
Absorption coefficient
Scattering coefficient
Scattering phase function
Light availability
Photobioreactor
Microalgae

ABSTRACT

Regardless if a kinetic expression of a light-dependent bioprocess is being sought, the parameters of that kinetic function are being adjusted, or a scaling-up process is being carried out to predict the productivity of a reactor, it is necessary to know the light availability in the culture volume. The emission characteristics of the radiation source, the geometry of the reactor as well as the optical properties of the suspension that resides within it must be known to achieve the latter. Here, we present an approach to quantify the optical properties of microalgae suspensions. A simple methodology, consisting in illuminating a suspension of microalgae with a characterised polychromatic radiation source and assessing how the directions are modified, and the amount of energy carried by the light beams after crossing the suspension, was successfully employed. Subsequently, through an optimisation program, the experimental culture data has been used to determine the spectral absorption and scattering coefficients of photons, and the suspension's scattering phase function. For a given microalgal culture, eight samples corresponding to a cultivation time of one week were analysed, utilising an energy balance, independently of the biomass or pigment concentration. Altogether the results presented here suggest that this methodology could be adapted to other suspensions, allowing accessible ways to evaluate the radiative characteristics of phototrophic microorganisms in the complex context of the evolution through time of the radiant energy field inside a photobioreactor.

List of symbols, abbreviations and units

PBR	photobioreactor
OP	optical property
REF	radiant energy field
RTE	radiative transfer equation
MC	Monte Carlo
PAR	photosynthetic active radiation
r_{abs}	local volumetric light absorption rate [μmol L^{-1} day^{-1}]
κ_λ	absorption coefficient [mm^{-1}]
σ_λ	scattering coefficient [mm^{-1}]
$\beta_{\theta,\lambda}$	the scattering phase function
$I'_\lambda(\hat{\Omega})$	the spectral intensity [μmol s^{-1} nm^{-1} sr^{-1}]
$I'^{*}_\lambda(\hat{\Omega})$	the spectral intensity of the sample [μmol s^{-1} nm^{-1} sr^{-1}]
$I^{R}_\lambda(\hat{\Omega})$	the relative spectral intensity
$I^{R,*}_\lambda(\hat{\Omega})$	the relative spectral intensity of the sample
$\hat{I}_R(\hat{\Omega})$	the average spectral intensity in the PAR spectral range
Q_λ	the total photon flux [μmol s^{-1}]
Q^*_λ	the total photon flux through the suspension [μmol s^{-1}]
$(Q^*_\lambda)_{GA}$	the total photon flux through the suspension (algorithm) [μmol s^{-1}]
$(Q^*_\lambda)_{EXP}$	the total photon flux through the suspension (experiment) [μmol s^{-1}]
$(\mu^*_m)_\lambda$	coefficient of the phase function [rad]
$(\bar{\mu}^*_n)_{PAR}$	averaged coefficient of the phase function in the PAR range [rad]

1. Introduction

Photobioreactors (PBRs) are the preferable units for the cultivation of photosynthetic microorganisms. Even if the culture is mixotrophic or

* Corresponding author at: Instituto de Desarrollo Tecnológico para la Industria Química (INTEC), Güemes 3450 (S3000GLN), Santa Fe, Argentina.
E-mail addresses: mibaniez@intec.unl.edu.ar (M.V. Ibañez), rleonardi@intec.unl.edu.ar (R.J. Leonardi), heinrichmiguel@hotmail.com (J.M. Heinrich), juliane.steingroewer@tu-dresden.de (J. Steingroewer), thomas_walther@tu-dresden.de (T. Walther), felix.krujatz@tu-dresden.de (K. Felix).

https://doi.org/10.1016/j.jpap.2020.100007
Received 30 June 2020; Received in revised form 8 September 2020; Accepted 3 October 2020
Available online 13 October 2020

autotrophic, light must reach the suspension passing through the unit's walls. Consequently, the optimisation and control of light transfer in PBRs are bound to the close relationship between the characteristics of the source of light, the geometry of the system and the radiative properties of the microorganisms dependent on the physiological state of the cell at any given time [1]. The combination of these three features in the radiative transfer equation (RTE) allows access to the radiant energy field (REF) in a PBR and, subsequently, the knowledge of the light availability inside the unit and the local volumetric rates of absorption of light (r_{abs}) in the photosynthetic active radiation (PAR) spectral range [2]. The absorption rates can be translated in growth rate values linked to a growth kinetic expression and further, the productivity of a particular configuration. Nonetheless, during the progression of a run, the radiant energy field in, and the composition of the liquid medium underlies a significant dynamic change. Thus photo-adaptative biological processes and physical-chemistry of the system might alter the radiation properties of the suspension, throughout variations in the composition of biomass and morphology of the cells, altering growth directly [3,4].

The spectral optical properties of the suspensions (OPs) are the absorption coefficient (κ_λ), the scattering coefficient (σ_λ) and the scattering phase function ($\beta_{\theta,\lambda}$). They account for a fraction of incoming light that is effectively absorbed, scattered and, in case of scattering, the distribution of a beam in a new direction around the previous one, respectively (Fig. 1(1.0)) [1]. Due to the heterogeneous and nonspherical nature of the cells, and the limited information concerning the radiative properties of intracellular constituents, numerous works have been published regarding its determination, explaining the interaction between cells with light as an equivalent homogeneous molecular medium that must reckon for the cells' internal heterogeneities [5,6, –7]. Microalgae are, whence, pictured as composite material whose volume is divided into organelles assuming a homogeneous refraction index and, a negligible scattering effect of separate molecules [8]. Then, complex refraction indexes of the suspension, which are dependent on wavelength and density of the material, stand for this simplification, composed of an imaginary part linked to the absorption behaviour and quantity of pigments present and the real part, which counts for the detailed description of the other non-absorbing cellular components, and usually is approximated.

The inclusion of different cell geometries and size distributions with experimental data such as biomass concentration, pigments content, normal-normal and normal-hemispherical spectral transmittance, in either analytical solutions or experimental approaches aimed to solve the RTE, have provided sets of refractive indexes, absorption and scattering cross-sections in the PAR region, as well as analytical or empirical models of phase functions whose parameters were regressed from experimental data. Although these OPs have been effectively used in the calculation of light availability inside a PBR unit, there is a lack of consensus about some discrepancies (i.e. nonlinear behaviour of pigments and adopted models regarding the cells' shape) previously reported [10,11]. The pigment molecules are modelled typically as be diluted enough to be characterised by an *in vivo* absorption cross-section and an internal pigment concentration. The latter leads to take the system as independent of the microorganism characteristics (cellular shape, metabolism) and become strongly dependent on the medium's chemical-composition and culture conditions. Consequently, the spectral absorption coefficients can be estimated, expressing it as the sum of *in vivo* previously reported absorption cross-sections under the PAR region, with a linear dependence on cells' pigments concentration [12]. However, due to the none considered biological aspects, it has been reported that a first-order approximation could not be accurate enough due to a 'package effect' of the pigments, supporting the fact that the OPs must be experimentally determined due to a potential lack of reproducibility [13]. As for the scattering phase function, making use of cell's size distribution models and experimental data, usually different expressions are employed, assuming forward scattering and dependence only on the azimuthal angles [5]. One of them was found to be nearly dependent on wavelength over the PAR region [11]. It was posited though, that the majority of the models are sufficient in predicting light absorption yet inaccurate regarding scattering distribution. Besides, it is not clear if there is no effect whatsoever of the polarised properties of the scattered light throughout the evolution of the REF [14].

Given the necessity of applying rigorous solutions upon these complex reflective systems, another published alternative to calculating the REF is the simulation of the radiation through Monte Carlo (MC) method, avoiding the inherent difficulties in solving the RTE [15,16]. This method emulates physical reality by tracking photons along their paths through an algal suspension. A huge advantage of such procedure relies on the premise that it enables the handling of the optical phenomena occurring within the suspensions and on their physical limits, with the characteristics of the light emitted by radiant energy sources (in direction and spectral composition) without the need of introducing simplifications to make the problem mathematically accessible [9]. Here the liquid medium must be treated as a continuum and, the cells are replaced as a homogeneous dispersion of absorption and scattering centres of energy. After firing a large number of photons from the source of light, the OPs are utilised then to track the steps of the photons flying in the suspension. These are different since the absorption and scattering probabilities assigned to the cells depend on the simulated wavelengths and their interaction with the ensuing OPs.

The present study aims to calculate the microalgae suspensions' OPs under the foundation that the pigment content and all of the non-absorbing components of individual cells are highly dynamic variables, however, overall these produce a particular REF in its interaction with the light, which holds for the photo-adaptative phenomena and environmental conditions of a unique moment (Fig. 1(1.0)). Cellular metabolism is not as fast as the radiative phenomena on which the OPs are involved. Thus, the evolution of the REF is here assessed, utilising an energy balance which reckons for the considerable variations in the medium's composition, including the inner structure and shape of the cell in the same model. Based on the latter, a simple methodology was employed, consisting of (i) the design and construction of a device that allows recording the values of the photon flux density through different angles with respect of the main emission direction of the radiation source; (ii) the characterisation of the light source's spectral and emission distribution functions; (iii) the development of an algorithm which allows the physical simulation of a system comprised by the light spring, the cuvette holding microalgae' suspension and the position and orientation of the detector; (iv) nest the algorithm obtained in (iii) inside a genetic algorithm to calculate the values of the radiative properties through the utilisation of recorded experimental data. By means of this methodology, eight sets of OPs over the PAR spectral region were obtained, corresponding to samples from a culture of *Chromochloris zofingiensis*, obtained through eight different times alongside a typical one-week batch culture. Since the methodology is based on an energy balance, it did not require the knowledge of the medium's composition, pigment content or microorganism' nature. Consequently, this method might be thought, as a more natural way of calculating the radiative properties of other microalgae suspensions in a faster and reliable way, designed for laboratory or industrial applications.

2. Materials and methods

2.1. Light emission and collection system

The source of light utilised in this work is a tungsten halogen HL-2000 lamp (Ocean Optics). The lamp's stable wavelength range is 360–2400 [nm], and it maximises light throughput with adjustable focus and alignment through an SMA 905 connector (Ocean Optics) with provides accuracy to the light collection of optical fibres.

The detector employed was a Red Tide 650 spectrometer (Ocean Optics). The spectrometer's resolution is 2 [nm] with a detectable spectrum ranged between from 350 to 1000 [nm]. The spectral data have been

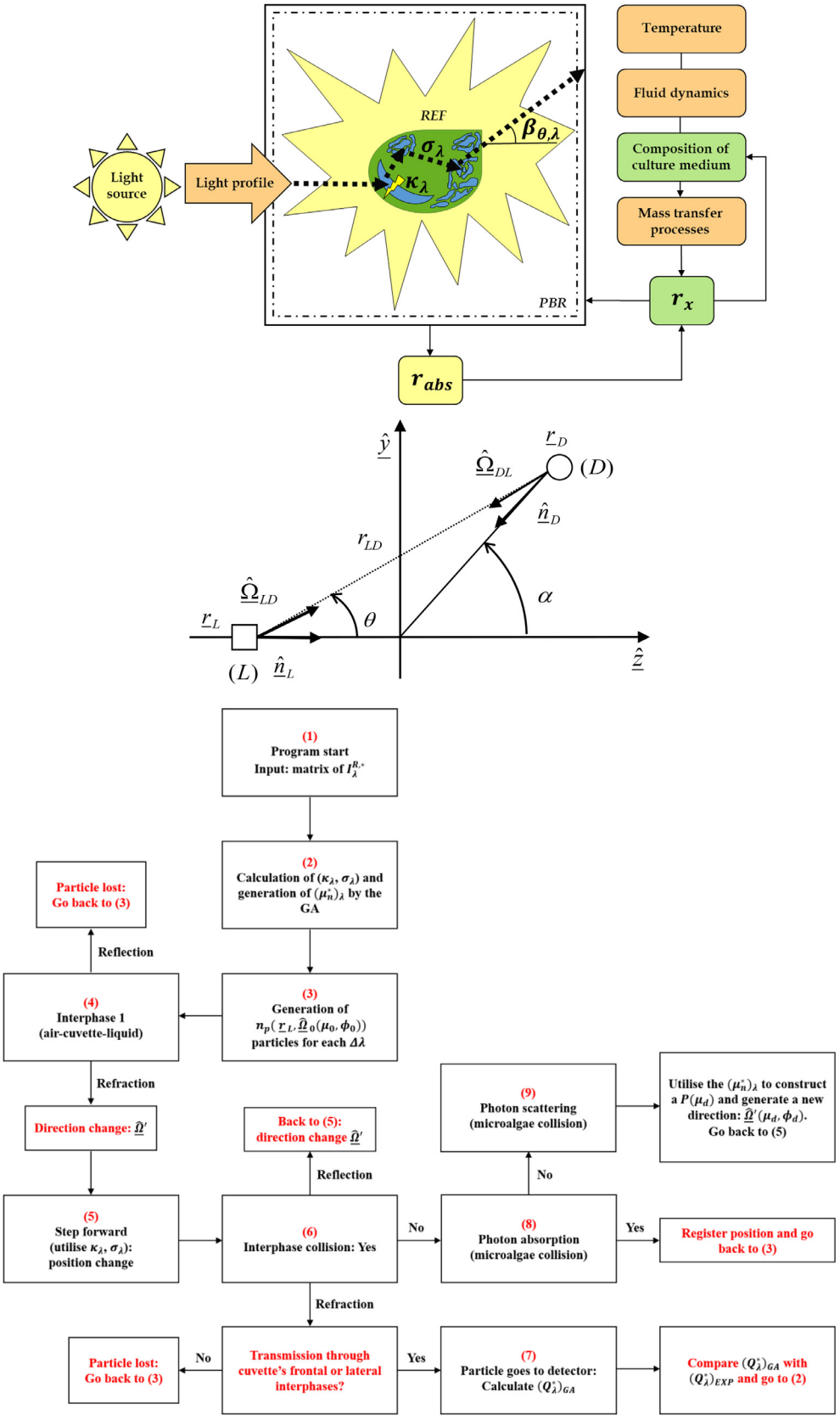

Fig. 1. (1.0): A PBR can be understood by treating per separate the three major components of the system: the light (yellow), the geometry of the system and operating conditions (orange) and every aspect concerning the microorganism present (green). The incident light in its interaction with the physical boundaries of the system generates a unique light profile. Further, the microalgae' OPs (κ_λ, σ_λ, $\beta_{\theta,\lambda}$) and the physicochemical system conditions in the interaction with this light profile creates the REF, which allows the calculation of r_{abs} and r_x for a particular moment alongside the cultivation time.
Fig. (1.1): Schematics of the 3D-printed device made of PA2200 with the correspondent reference system and the two optical fibres with the cuvette.
Fig. (1.2): Schematics of the device. Geometrical definition of the system employed.
Fig. (1.3): Computational flowchart, including the decision nodes in the stochastic algorithm developed for the Monte Carlo simulation of the REF inside the PBR.

obtained employing a software provided by the manufacturer, SpectraSuite (Ocean Optics). The latter was configured with the lowest integration time and default options disabled.

The optical fibres used were two pieces of stainless steel QP50-2-UV-BX fibres (Ocean Optics), with a robust transmission capacity from 300 to 1100 [nm] and 50 [um] diameter size.

2.2. Strain and cultivation conditions

The batch cultivation of *Chromocloris zofingiensis SAG 221-2* (SAG – Göttingen) was performed in a 100 [L] tubular photobioreactor of MINT Engineering GmbH (Dresden, Germany). The PBR has 19 plastic tubes with an inner diameter of 0.57 [m] and length equal to 1.4 [m]. The liquid circulates with a pumping rate of 1 [L min^{-1}] and air and CO_2 gassing rates of 5 10^{-5} and 2.5 10^{-6} [vvm] respectively. The CO_2 input was utilised to maintain the pH level in a value equal to 7. The temperature was fixed in 23 [°C]. A concentrated inoculum was prepared in an illuminated chamber to start the cultivation with a biomass concentration equal to 0.1 [g L^{-1}] in exponential phase.

The culture medium employed either for the inoculum or the PBR is BM, with the following composition: $NaNO_3$– 7.5 10^{-1} [g L^{-1}], $MgSO_4.7H_2O$ – 7.5 10^{-2} [g L^{-1}], $CaCl_2.2H_2O$ – 2.5 10^{-2} [g L^{-1}], K_2HPO_4– 7.5 10^{-2} [g L^{-1}], KH_2PO_4– 1.75 10^{-1} [g L^{-1}], NaCl – 2.5 10^{-2} [g L^{-1}], $ZnSO_4.7H_2O$ – 2.87 10^{-4} [g L^{-1}], H_3BO_3– 6.10 10^{-5} [g L^{-1}], $MnCl_2.6H_2O$ – 1.69 10^{-4} [g L^{-1}], $CuSO_4.5H_2O$ – 2.5 10^{-6} [g L^{-1}], $(NH_4)_6Mo_7O_{24}.7H_2O$ – 1.24 10^{-6} [g L^{-1}] and $FeCl_3.6H_2O$ – 5 10^{-3} [g L^{-1}].

2.3. Experimental set-up

The experimental set-up was composed of a light source, a detector, two optical fibres connected to both devices and the other edge of the fibres into a plastic 3D-printed device (Fig. 1(1.1)). The latter is a semicircle of 0.1 [m] of diameter made of PA2200, which holds a space for a rectangular custom made cuvette sized: (0.028 × 0.028 × 0.0025) [m]. On the left-hand side of the cuvette, there is a hole designed for holding an optical fibre, which carries the light coming from the light source. On the right-hand side, there is a mobile holder, designed for the detector's optical fibre, whose position can be adjusted throughout different equidistant marks placed on the semicircle's surface, from 0 to 180°, each 2.5°. The two holders are aligned to ensure proper measurement (Appendix – Fig. (1a–c)).

Every measurement was performed filling the cuvette with 2 [mL] of culture and utilising the intensity-recording function of the SpectraSuite software (Ocean Optics). The spectral intensity of each sample $I'^{*}_{\lambda}(\hat{\Omega})$ (Section 3.1) was then calculated as the average of three different spectra each 2.5°, starting in the zero position taken as the total alignment of both optical fibres, and recording the spectral data from 0° to 90°, and further 0° to −90°. With every averaged sample's continuous spectrum, 31 intervals of $\lambda \pm 5.0$ [nm] were considered for each angle, corresponding to the spectral range $400 \leq \lambda \leq 700\,[nm]$. Further, each one of these 31 dependencies was divided by $I'_{\lambda}(\mu = 1)$, the spectral intensity of the two fibres fully aligned (Sections 3.1 and 3.2), allowing to obtain the normalised relative spectral intensity of the sample $I^{R,*}_{\lambda}(\mu)$, for each angle and each one of the 31 wavelength intervals. Finally, through the system's symmetry, it was calculated the average of the $I^{R,*}_{\lambda}(\mu)$correspondent to each one of the positive and negative angles into one unique value of relative spectral intensity in the range from 0° to 90° for each PAR spectral interval under study. The latter bestowed the construction of a matrix of $I^{R,*}_{\lambda}(\mu)$, with many columns corresponding to the number of considered angles, and 31 rows related to each wavelengths' interval.

As for the system's calibration, the different continuous spectra were recorded only for the ensuing relative spectral intensities in every angle without the cuvette. Every matrix has then utilised in an optimisation routine (Fig. 1(1.2)) to obtain the values of the samples' radiative properties. All the regressions were performed utilising the *lscqcurvefit* solver of Matlab. The latter is a nonlinear least-squares solver that finds the coefficients necessary to minimise the difference between observed data and input data. Every independent data series was adjusted utilising the trust-region-reflective algorithm, under a default step tolerance and function tolerance. Finally, the nonlinear 90% confidence intervals of any calculated parameter of interest were calculated through *nlparci* solver of Matlab. This last required the Jacobian matrix of the regression of each experimental data series obtained.

3. Theoretical approach and mathematical model

In this section, the mathematical basis that allows the calculation of the absorption coefficients (κ_{λ}), scattering coefficients (σ_{λ}) and the scattering phase function ($\beta_{\theta,\lambda}$) is described. The first step is to define the energy exchange between the detector (D) and the source of light (L), which grants the access to calculate the total photon flux independently from the receiving surface, with or without another element among them (i. e. the system can be used with or without a cuvette with a phototropic suspension inside). Later, these definitions are further employed to define the directional probability functions linked to the experimental data and, last but not least, the simulation of the different tracks of the light and its interaction with the particles are explained as part of the subroutine which works with the MC method. Making use of the equations defined in the first part the latter brings the feedback loop to a genetic algorithm, which reproduces the experiment, creating a scattering phase function whose coefficients are bounded to the experimental data with the $t\,\kappa_{\lambda}$ and σ_{λ} previously calculated.

3.1. The radiant energy emission by the light source

The number of photons ΔE^{LD}_{λ} with a wavelength corresponding within the range $\lambda + \Delta\lambda$, which arrives at (D) coming from (L) (Fig. 1(1.2)) during an interval of time Δt, can be known through utilising the radiant energy exchange equation [26]:

$$\Delta E^{LD}_{\lambda} = I_{\lambda}\left(\hat{\Omega}\right)\Delta\lambda\Delta t\frac{A_L\left(\hat{n}_L\cdot\hat{\Omega}_{LD}\right)A_D\left(\hat{n}_D\cdot\hat{\Omega}_{DL}\right)}{r^2_{LD}} \tag{1}$$

In Eq. (1), $I_{\lambda}(\hat{\Omega})$ is the emission source spectral Irradiadiance [μmol s^{-1} m^{-2} sr^{-1} nm^{-1}]; A_D y A_L the areas of (D) and (L) [m^2]; r_{LD} is the distance between (D) and (L) [m]; Δt is the duration of the energy exchange over time [s]; $\Delta\lambda$ is the wavelength range considered [nm]; $\hat{\Omega}_{LD}$, and $\hat{\Omega}_{DL}$ are directional unitary vectors corresponding to (D) and (L); and, $\hat{n}_L$ and $\hat{n}_D$ are the normal vectors of each flat surface.

Further rearrangement of Eq. (1) allows the calculation of the spectral photon flux density $q^{D}_{\lambda,\alpha}$ [μmoles s^{-1} m^{-2} nm^{-1}] which arrives at (D) in terms of the angle α and, the respective distance between the origin and, (L) and (D), d_L and d_D [m] respectively (Fig. 1(1.2)):

$$q^{D}_{\lambda,\alpha} = \frac{\Delta E^{LD}_{\lambda}}{\Delta t\Delta\lambda A_D} = I_{\lambda}\left(\hat{\Omega}\right)A_L\frac{\left(\hat{n}_L\cdot\hat{\Omega}_{LD}\right)\left(\hat{n}_D\cdot\hat{\Omega}_{DL}\right)}{r^2_{LD}} \tag{2.1}$$

$$r_{LD} = \left|\underline{r}_{LD}\right| \tag{2.2}$$

$$\underline{r}_{LD} = \underline{r}_D - \underline{r}_L \tag{2.3}$$

$$\underline{r}_L = -d_L\underline{\hat{z}} \tag{2.4}$$

$$\underline{r}_D = d_D\cos\alpha\,\underline{\hat{z}} + d_D\sin\alpha\,\underline{\hat{y}} \tag{2.5}$$

If we consider A_L sufficiently smaller in comparison with A_D (differential surface), it is possible to call $I'_{\lambda}(\hat{\Omega})$ to the number of photons that are emitted from (L) per unit of time, wavelength and solid angle [μmol s^{-1} nm^{-1} sr^{-1}], accounting for the light source surface. Then,

$I'_\lambda(\underline{\hat{\Omega}})$ can be assessed through:

$$I'_\lambda\left(\underline{\hat{\Omega}}\right) = I_\lambda\left(\underline{\hat{\Omega}}\right)A_L = \frac{q^D_{\lambda,\alpha} r^2_{LD}}{\left(\underline{\hat{n}}_L \cdot \underline{\hat{\Omega}}_{LD}\right)\left(\underline{\hat{n}}_D \cdot \underline{\hat{\Omega}}_{DL}\right)} \tag{3}$$

Additionally for our purposes, with the definition of a solid angle:

$$\Delta\underline{\hat{\Omega}}_D = \frac{A_D\left(\underline{\hat{n}}_D \cdot \underline{\hat{\Omega}}_{DL}\right)}{r^2_{LD}} = \sin\theta\Delta\theta\Delta\phi = -\Delta\cos\theta\Delta\phi \tag{4}$$

Eq. (1) can be rewritten in the following way to achieve a different shape of Eq. (2):

$$\begin{aligned}\Delta E^L_{\lambda,\underline{\hat{\Omega}}} &= I_\lambda\left(\underline{\hat{\Omega}}\right)A_L\Delta t\Delta\lambda\left(\underline{\hat{n}}_L \cdot \underline{\hat{\Omega}}_{LD}\right)\frac{A_D\left(\underline{\hat{n}}_D \cdot \underline{\hat{\Omega}}_{DL}\right)}{r^2_{DL}} \\ &= -I'_\lambda\left(\underline{\hat{\Omega}}\right)\Delta t\Delta\lambda\left(\underline{\hat{n}}_L \cdot \underline{\hat{\Omega}}_{LD}\right)\Delta\underline{\hat{\Omega}}_D\end{aligned}$$

$$Q^L_{\lambda,\underline{\hat{\Omega}}} = \frac{\Delta E^L_{\lambda,\underline{\hat{\Omega}}}}{\Delta t\Delta\lambda} = I'_\lambda\left(\underline{\hat{\Omega}}\right)\left(\underline{\hat{n}}_L \cdot \underline{\hat{\Omega}}\right)\Delta\underline{\hat{\Omega}} \tag{5}$$

The final shape of Eq. (5) grants the calculation of the spectral photon flux $Q^L_{\lambda,\underline{\hat{\Omega}}}$ [μmoles s^{-1} m^{-2} nm^{-1}] with a direction corresponding to the range $\underline{\hat{\Omega}}$ and $\underline{\hat{\Omega}} + \Delta\underline{\hat{\Omega}}$. The replacement of $\Delta\underline{\hat{\Omega}}$ by $-\Delta\phi\Delta\cos\theta$, $(\underline{\hat{n}}_L \cdot \underline{\hat{\Omega}})$ by $\cos\theta$ and computing the limit of Eq. (5) under $\Delta\cos\theta \to 0$ and $\Delta\phi \to 0$; gives:

$$dQ^L_{\lambda,\underline{\hat{\Omega}}} = -I'_\lambda\left(\underline{\hat{\Omega}}\right)\cos\theta d\cos\theta d\phi = -I'_\lambda\left(\underline{\hat{\Omega}}\right)\mu d\mu d\phi \tag{6}$$

In Eq. (6), $\cos\theta$ was replaced by μ for the sake of simplifying. Finally, *the total spectral photon flux* across every ϕ and θ possible directions is:

$$\begin{aligned}Q_\lambda &= -\int_0^{2\pi}\int_1^0 I'_\lambda\left(\underline{\hat{\Omega}}\right)\mu' d\mu' d\phi' = \int_0^{2\pi} d\phi' \int_1^0 I'_\lambda(\mu')\mu' d\mu' \\ &= 2\pi\int_0^1 I'_\lambda(\mu')\mu' d\mu'\end{aligned} \tag{7}$$

3.2. The photon emission probability in the directions $\hat{\Omega}(\theta,\phi)$

The differential probability that a photon during the emission was emitted in one direction μ is:

$$dP(\mu) = \frac{dP(\mu)}{d\mu}d\mu = \xi(\mu)d\mu \tag{8}$$

In Eq. (8), $\xi(\mu)$ is the distribution function of photon emission probabilities in different directions. Then, the cumulative probability that said photon has been emitted in a direction between 1 and μ can be calculated and, at the same time, this probability can be though as the fraction of emitted photon flux within the range $1<\mu'<\mu$:

$$P(\mu) = \int_1^\mu \xi(\mu')d\mu' = \frac{\int_0^{2\pi}\int_1^\mu dQ^L_{\lambda,\underline{\hat{\Omega}}}}{\int_0^{2\pi}\int_1^0 dQ^L_{\lambda,\underline{\hat{\Omega}}}} = \frac{\int_1^\mu I'_\mu(\mu')\mu' d\mu'}{\int_1^0 I'_\lambda(\mu')\mu' d\mu'} \tag{9}$$

Moreover, to evaluate if the emitted light has the same directional distribution over the wavelength, it is useful to calculate *the relative spectral intensity* $I^R_\lambda(\underline{\hat{\Omega}})$, relative to the relation among the different $I'_\lambda(\underline{\hat{\Omega}})$, divided by $I'_\lambda(\mu = 1)$ (i. e. $I'_\lambda(\theta = 0)$). Inasmuch as the latter is valid, Eq. (9) can be reshaped to:

$$P(\mu) = \frac{\int_1^\mu I^R_\lambda(\mu')\mu' d\mu'}{\int_1^0 I^R_\lambda(\mu')\mu' d\mu'} \tag{10}$$

Eq. (10) can, whence, be solved by numerical integration from the $I^R_\lambda(\mu)$ values obtained experimentally. As for $\xi(\mu)$, the probabilities can be calculated utilising Eq. (8) as the derivative of $P(\mu)$ concerning μ.

As for the ϕ component angles, every direction is possible to be selected; thus:

$$\xi(\phi) = \frac{1}{2\pi} \text{ and subsequently, } P(\phi) = \frac{1}{2\pi}\int_0^\phi d\phi' = \frac{\phi}{2\pi} \tag{11}$$

3.3. The interaction of the light with the phototrophic suspension

In this study, a stochastic algorithm based on the Monte Carlo method is devised for the simulation of the REF in the algal suspensions, the methodology developed and described by Heinrich et al. [1,3]. The simulated experiment starts generating a total quantity of photons $n_p(\underline{r}, \underline{\hat{\Omega}}, \lambda)$ coming from the light source. These moves through the PBR walls and phototrophic suspension like a nonuniform gas at light speed, in varying directions. For each value in the spectral range: $400 < \lambda + 10 < 700$ [nm], the fate of the algorithm is to produce 31 dependencies of *the relative spectral intensity through the suspension*, $I^{R,*}_\lambda(\mu)$, reproducing the experiment for the 31 $n_p(\underline{r}, \underline{\hat{\Omega}}, \lambda)$ photon densities composing each wavelength under study. Each one of the photons starts with the position $\underline{r}_L$ Fig. 1(1.2)) and with an initial direction $\underline{\hat{\Omega}}_0(\mu_0, \phi_0)$. The latter is provided through the generation of two random numbers δ_μ and δ_φ, between 0 and 1, and the use of the known $P(\mu)$and $p(\phi)$ functions (Eqs. (10) and ((11)). Then, the reflectivity on the interface between air and the culture medium$\rho_{1,2}$ is computed according to Fresnel's law [3].

Once each photon is inside the phototrophic continuous suspension, their respective trajectories are described on a probabilistic base. These pathways might be deflected by scattering effects due to elastic interactions between photons and suspended cells, or even reach a sudden end due to absorption. The algorithm requires the radiative properties (κ_λ, σ_λ, $\beta_{\theta,\lambda}$) to simulate these events. In this approach, these were provided by the genetic algorithm (GA) employed (Fig. 1(1.3). Therefore, κ_λ and σ_λ are calculated with the matrix of spectral intensity, and a set of parameters belonging to $\beta_{\theta,\lambda}$ are created to reproduce each $I^{R,*}_\lambda(\mu)$ under analysis, respecting the following expressions:

$$\left(\kappa_\lambda + \sigma_\lambda\right) = \frac{-\log\left(\frac{I^{R,*}_\lambda(\mu=1)}{I^R_\lambda(\mu=1)}\right)}{d_C} \tag{12}$$

$$\kappa_\lambda = \frac{-\log\left(\frac{\int_1^0 I^{R,*}_\lambda(\mu')\mu' d\mu'}{\int_1^0 I^R_\lambda(\mu')\mu' d\mu'}\right)}{d_C} \tag{13}$$

In Eq. (12), the term $\frac{I^{R,*}_\lambda(\mu=1)}{I^R_\lambda(\mu=1)}$ is the division among the value of the relative spectral intensity with, and without cuvette in the system, accounting for $\theta = 0$. d_C is the narrow optical path of the cuvette [m]. The term $\frac{\int_1^0 I^{R,*}_\lambda(\mu')\mu' d\mu'}{\int_1^0 I^R_\lambda(\mu')\mu' d\mu'}$ in Eq. (13) represents the division between the total emitted energy from the light source with, and without cuvette, respectively.

Regarding the scattering phase function, under this model $\beta_{\theta,\lambda}$ is meant as the differential probability function (i. e. same in shape as Eq. (8)) which allows the assessment of the most probable azimuthal angles that the photons might take after expe-

riencing the event of scattering, following the next procedure:

1) Generation of angles by GA

$$\mu_1^* = 1 \quad (14.1)$$

$$\mu_2^* = \mu_1^*\mu_2^* \quad (14.2)$$

$$\mu_3^* = \mu_2^*\mu_3^* \quad (14.3)$$

$$\mu_4^* = \mu_3^*\mu_4^* \quad (14.4)$$

$$\mu_5^* = \mu_4^*\mu_5^* \quad (14.5)$$

$$\mu_6^* = \mu_5^*\mu_6^* \quad (14.6)$$

2) Generation of a random number

$$0 \leq \delta_\beta \leq 1$$

3) Construction of $\delta_\beta = P(\mu_d)$

$$0.0 \leq P(\mu_d) \leq 0.2 \qquad \mu_d = \mu_1^* - \delta_{\mu^*}[\mu_1^* - \mu_2^*] \quad (15.1)$$

$$0.2 < P(\mu_d) \leq 0.4 \qquad \mu_d = \mu_2^* - \delta_{\mu^*}[\mu_2^* - \mu_3^*] \quad (15.2)$$

$$0.4 < P(\mu_d) \leq 0.6 \qquad \mu_d = \mu_3^* - \delta_{\mu^*}[\mu_3^* - \mu_4^*] \quad (15.3)$$

$$0.6 < P(\mu_d) \leq 0.8 \qquad \mu_d = \mu_4^* - \delta_{\mu^*}[\mu_4^* - \mu_5^*] \quad (15.4)$$

$$0.8 < P(\mu_d) \leq 1.0 \qquad \mu_d = \mu_5^* - \delta_{\mu^*}[\mu_5^* - \mu_6^*] \quad (15.5)$$

In Eqs. (14.1)–(14.6), the $(\mu_n^*)_\lambda$ coefficients are azimuthal angles generated by the GA in such a way that from $(\mu_1^*)_\lambda$ to $(\mu_6^*)_\lambda$, the probability of occurrence of each generated angle is decreasing or, in other words, the most favoured directions to be selected are the ones in the surroundings of $(\mu_d)_\lambda = 1$ (i. e. $\theta = 0$). A function $P(\mu_d)$, which is bounded to fulfil this feature, represents a $\beta_{\theta,\lambda}$ function in a forward scattering scenario, which is appropriate for the analysis of the light interaction with particles holding sizes similar to the magnitude of the incident wavelength over them [8]. The new $\hat{\Omega}'(\mu_d, \phi_d)$ direction is provided then by Eqs. (15.1)–(15.6) making use of a random number δ_{μ^*} and, a polar angle provided by a dependence similar to Eq. (11).

After a succession of scattering events, the particles which were not removed from the light field have the chance to pass through the physical boundaries of the cuvette and, if they are not reflected inside again, they continue its way to reach the detector. Eq. (3) is used then to calculate the ensuing $I_\lambda'^*(\mu)$, and after using $I_\lambda'(\mu = 1)$, the corresponding $I_\lambda^{R,*}$. Finally, making use of Eq. (9) *the total photon flux through the suspension* $(Q_\lambda^*)_{GA}$ is calculated by the subroutine who works employing the MC method. The latter is given to the GA, thereby allowing the comparison with the experimental total photon flux previously measured $(Q_\lambda^*)_{EXP}$ and the estimation of the absolute error to start again with the next evolution of the coefficients from Eqs. (15.1) to (15.6). The best fit of the GA is, whence, the result of Eqs. (14.1)–(14.6) which allows the best estimation of $(Q_\lambda^*)_{EXP}$, fulfilling the restriction imposed by Eqs. (12) and (13).

4. Results and discussion

The optimisation and control of light transfer in PBRs on which an autotrophic process is carried out, are bound to the close relationship between the radiation source's emission characteristics, the geometry of the reactor as well as the optical properties of the suspension that resides within it. The combination of these three components in the radiative transfer equation (RTE) allows access to knowledge the light availability inside the unit, which accounts for the physiological state of the culture in a given time. Since photo-adaptative biological processes and physical-chemistry of the system alters during the progression of a run, it is necessary to assess the changes over these radiative properties throughout time. A model of interaction linking light and the culture must be applied to do so, and due to the system's complexity, there is up to date a lack of agreement between the different empirical approaches, and still, there are no studies where both the inner structures and the shape of the cell are included to the model when describing algal cells with complex shapes.

Here, we present an approach to measure the optical properties of microalgae suspensions based on the simulation of the radiation employing Monte Carlo method. The advantage of the latter is that it allows handling complex reflexive systems and the optical phenomena occurring within it, without introducing simplifications to solve complicated mathematical approaches. Under this perspective, the culture is a continuum and, the cells are centres of absorption and scattering with associated probabilities accounting for these events. Below the assumption that detectable changes in light passing through the culture are faster in comparison with the biological processes involved in the progressive changes of the OPs, a simple methodology has been proposed, consisting in illuminating a *C. zofingiensis* suspension with a characterised polychromatic radiation source and assessing how the directions were modified, and the amount of energy carried by the light beams after crossing the suspension. Subsequently, through an optimisation program, the experimental culture data will be used to determine the spectral absorption and scattering coefficients of photons, and the phase function of the suspension. Collectively, the results presented here are independent on pigments' concentration and biomass' concentration, suggesting that this methodology allows more intuitive ways of calculating the radiative characteristics of phototrophic microorganisms in the complex context of the evolution through time of the radiant energy field inside a photobioreactor.

4.1. Simulation of the source of light

In the present work, a system composed of a polychromatic source of light, two optical fibres, meant for carrying the source's light and collecting it, respectively, and a spectrometer was placed upon a 3D-printed device made from PA2200 to quantify the radiative properties of a suspension of a phototrophic microorganism. The light modelling of a similar system, on which the photons move at lightspeed like a gaseous fluid, and the corresponding resolution of the RTE were published in previous reports [17]. The application of the Monte Carlo method over this system to solve an energy balance required first the knowledge of the light source spectral distribution, and the directional distribution of the emitted wavelengths. The latter has been evaluated here utilising the average relative spectral intensity $\overline{I}_R(\hat{\Omega})$ values, obtained as the average of the ensuing $I_\lambda^R(\hat{\Omega})$ quantities in the spectral range $400 < \lambda + 10 < 700\,[nm]$. Fig. 2 shows the $I_\lambda'(\hat{\Omega})$ registered values inherent to the HL-2000 lamp Eq. (3)) and Fig. 3 display the $\overline{I}_R(\hat{\Omega})$ corresponding to 11 angles in the range: $0.9 < \mu < 1$. While the light source's spectral emission is not homogeneous, the wavelengths' directions on the PAR spectral range are. Likewise, since the directional distribution must fulfil with Eqs. (9)

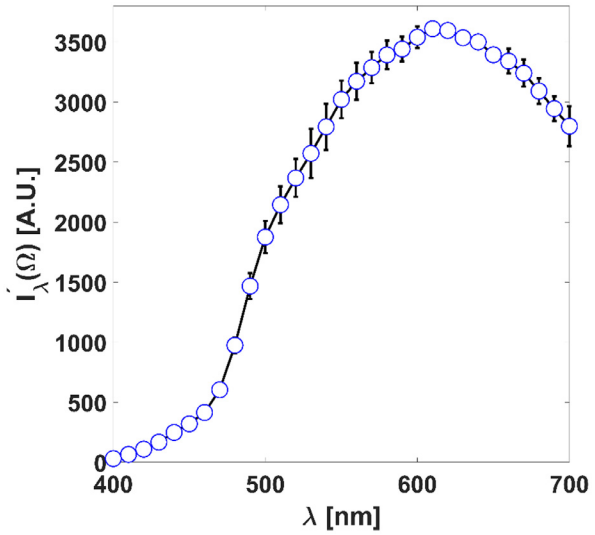

Fig. 2. Light source continuous spectra of the HL-2000 Halogen lamp obtained in the spectral range $400 < \lambda + 10 < 700\,[nm]$. The (○) blue dots are the ensuing spectral intensity values obtained for the PAR spectral region with the spectrometer RedTide 650. The acquisition of experimental data was performed through the measurement of ten spectra. The black error bars are the standard deviation of these average spectra (blue dots) with a 90% confidence interval.

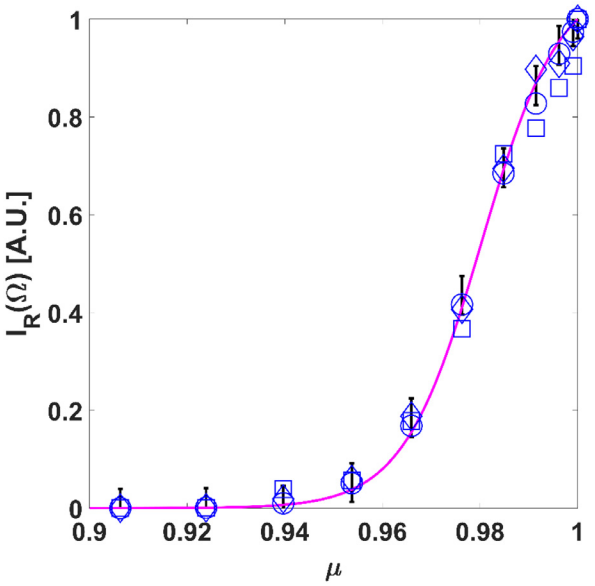

Fig. 3. Corresponding average relative intensity and its directional distribution concerning the azimuthal angles. The (○,□,◇) blue dots are the triplicate of the same experience performed in the light source simulation. The magenta line with black error bars is the continuous distribution regressed making use of Eq. (16) with a 90% confidence interval.

and ((10), the following expression valid for the range $0 < \mu < 1$ and $0 < \overline{I}_R(\hat{\underline{\Omega}}) < 1$ has been employed:

$$\overline{I}_R\left(\hat{\underline{\Omega}}\right) = \frac{a_1 - a_2}{1 + e^{\frac{\mu-\mu_0}{\delta}}} + a_2 \tag{16}$$

In Eq. (16), a_1, a_2, μ_0 y δ are four regressed parameters, with values: $0.00 \pm 2.30\ 10^{-2}$, $1.08 \pm 2.49\ 10^{-2}$, $9.80 \pm 2.25\ 10^{-2}$, $8.02\ 10^{-3} \pm 1.84\ 10^{-4}$. The latter allowed the simulation of the light source emission on the printed device (Fig. 3), and the reproduction of the $\overline{I}^*_R(\hat{\underline{\Omega}})$ values obtained with, first the empty cuvette present, and further with the cuvette and de-ionised water inside. Finally, the application of Eq. (7) over $\overline{I}_R(\hat{\underline{\Omega}})$, and $\overline{I}^*_R(\hat{\underline{\Omega}})$ quantities facilitated the estimation of Q_{PAR}, and Q^*_{PAR} correspondingly (Appendix – Table 2). In the case of the Fig. 2, the acquisition of experimental data was performed through the measurement of ten spectra. The dots in this figure are the average values of these spectra, and the error bars are the standard deviation of these magnitudes with a 90% confidence interval. For the case of the Fig. 3, the procedure has been the same, except for the data series, since only three series of data have been acquired, and the values presented are the average relative spectral intensities (The (○,□,◇) blue dots by triplicate), with their corresponding standard deviations of the mean of these experimental values (error bars with 90% confidence interval).

The total light source flux is required later for the application of Eq. (13), taking the value of $2.91\ 10^{-4} \pm 2.78\ 10^{-5}$ [μmol s^{-1}]. The reproducible Q^*_{PAR}values of the experiences with the empty cuvette, and with pure water were $2.82\ 10^{-4} \pm 2.64\ 10^{-5}$ [μmol s^{-1}] and $2.53\ 10^{-4} \pm 2.56\ 10^{-5}$ [μmol s^{-1}], 3% and 13% lower than Q_{PAR} on an individual basis.

4.2. Absorption and scattering coefficients of a suspension of a phototrophic microorganism

C. zofingiensis is a member of the Chlorophyta microalgae family. In recent years this strain has been used as a model for the study of the carotenoids biosynthetic pathway since it is possible to isolate from its interior either primary pigments like chlorophyll, *α*- and *β*-carotene, subsequently, lutein and violaxanthin under standard growth conditions, and secondary pigments as astaxanthin and canthaxanthin under stress conditions [18]. As for its potential as an industrially relevant alga, *C. zofingiensis* can assimilate different carbon sources, and it might produce proper astaxanthin and lutein levels with a robust, specific growth rate, either in an autotrophic cultivation mode or in the dark [19]. Under nutrient limiting conditions, it was found that this strain also produces high lipid content, pointed as a promising feedstock for biodiesel production [19]. Therefore, there is a severe concern about the development of tools for the scaling-up of this microorganism.

In *C. zofingiensis,* depending on the culture conditions, it was found that the size of the cells can vary from 4 to 9 [μm] (Appendix – Fig. 2), whether if the lighting conditions change in quality and quantity, or there are organic carbon sources present in the liquid [20]. The quantity and size of chloroplasts can also change in response to the environment in this strain, exhibiting larger photosynthetic starch storage capacity and changes in the carbon concentrating mechanisms [20]. Likewise, lipid accumulation may take place by the overexpression of acetyl-CoA carboxylase and the degradation of chlorophyll *a* and *b* [20]. Concomitantly, astaxanthin lipid bodies are synthesised outside chloroplasts, designed for photoprotection, as well as phenolic compounds which increase the overall antioxidant activity, among other components [20]. Although there are no studies so far related to the influence of the light stratification over *C. zofingiensis*, as this phenomenon appears with the growth in biomass quantity and the latter modify the REF, changes in the architecture and composition of photosystems might happen like in other members of the Chlorophyta family [17].

Here we sought to investigate the radiative properties of a *C. zofingiensis* phototrophic culture based on an energy balance. The latter allows the construction of a continuum medium of radiation properties in the culture volume in a single period, although unevenly distributed in space and wavelength. Then, the OPs which are related to the REF at this moment, fated to every chemical or biological alteration in the system, like the ones mentioned in previous paragraphs, were calculated under the restrictions imposed by Eqs. (12), (13) and (14-1), (6). In Fig. 4(a,d), eight sets of κ_λ and σ_λ coefficients in the PAR spectral range are presented. The trend in the coefficients' variations in the wavelengths region from 400 to 700 [nm] has shown expectable results in comparison with other members of Chlorophyta [10].

As for absorption, there are larger values at those wavelengths were the chlorophyll pigments are active to light. Free Chl *a* absorb around

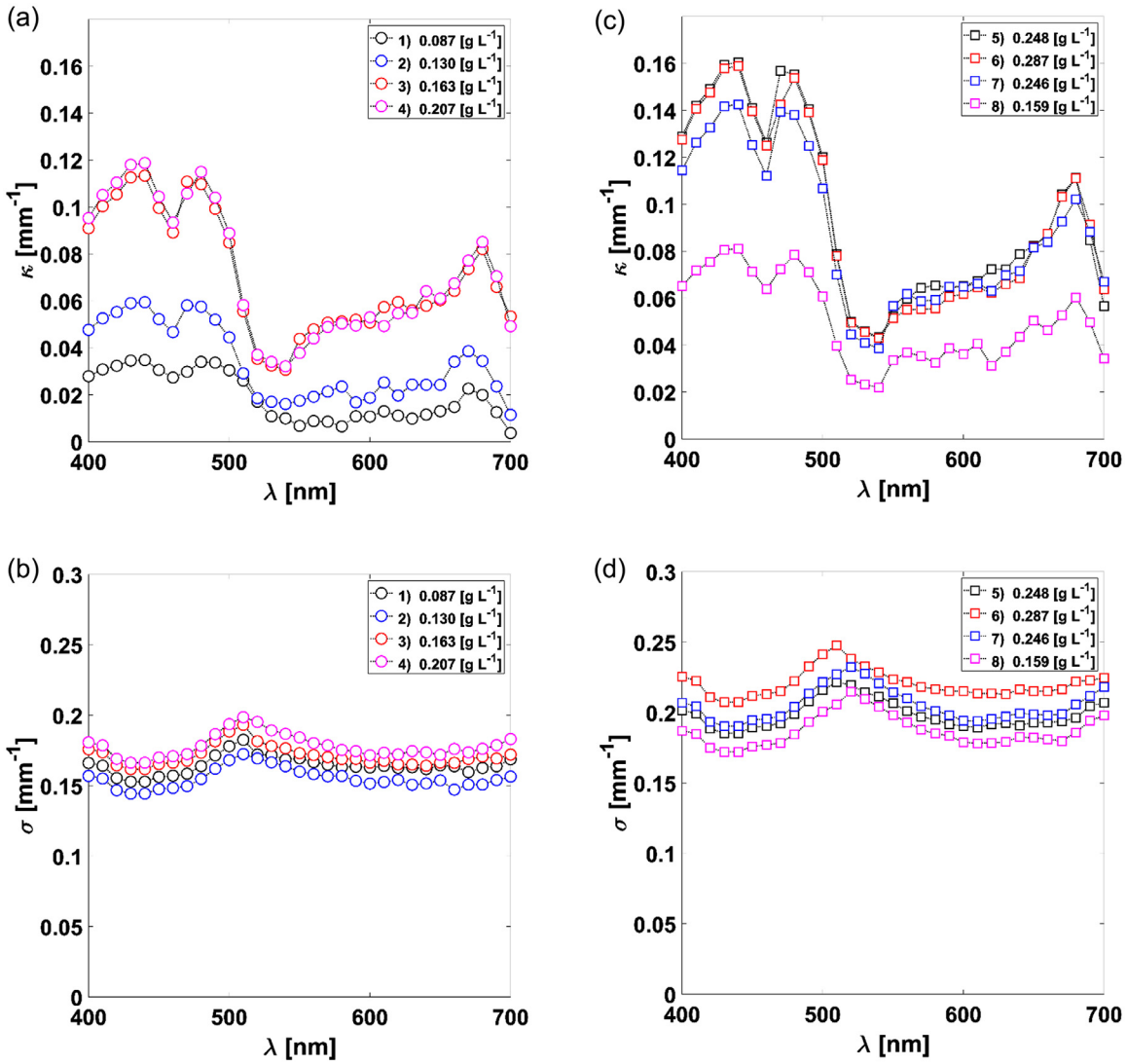

Fig. 4. (a,d): The absorption and scattering coefficients of eight samples. The (○) black, red, blue and magenta dots are correspondent with the $\kappa_\lambda$of samples 1–4 (Fig. (4-a)) and $\sigma_\lambda$respectively (Fig. (4-b)). The (□) black, red, blue and magenta dots are correspondent with the $\kappa_\lambda$of samples 5–8 (Fig. (4-c)) and $\sigma_\lambda$respectively (Fig. (4-d)).

435 and 676 [nm] while free Chl *b* present maxima peaks around 475 and 650 [nm] [5]. In Fig. (4-a) and (4-c) these peaks are smoother and present shifts due mainly to two effects: firstly, Chl molecules are supported by other proteins in the core antennas of the light-harvesting complexes in chloroplasts, which creates an overlapping in the spectrum of these free substances; secondly, as it was mentioned before, it is natural in *C. zofingiensis* the synthesis of carotenoids and xanthophylls [18]. Lutein and astaxanthin, as a representative of all the different α- and β-carotene intermediates, have absorption maxima around 445 and 474 [nm], and 480 [nm] on an individual basis [5,25]. The latter as well contribute to the spectral peaks overlapping alongside the PAR spectral range, which also explain the other variations present in the wavelengths range from 550 to 650 [nm].

Regarding the fate of the non-absorbed light, when absorption occurs in the LHC and the amplitude of an electromagnetic field changes, its phase will change accordingly, producing inelastic scattering. From Fig. (4-b) and (4-d) it can be observed the habitual trending in light dispersion's behaviour for a phototrophic suspension. Light scattering tends to be higher than microalgae absorption efficiency [21]. Even though the σ_λ coefficients depends on wavelength as the κ_λ coefficients, this wavelength-selectivity is not as sharp for the microalgae scattering spectrum. The latter may be attributed to the dominant influence of the non-absorbing cell components over the σ_λ, although pigments exert an effect through fluorescence and selective absorption [8]. The ensuing σ_λ to the spectral range 500–560 [nm] are the highest values (Fig. 4-c and 4-d), corresponding to the lowest κ_λ in Fig. (4-a) and (4-c), except for κ_{500} and κ_{510} which reckons for carotenoids nature in each sample. As for the two dips present in the blue and red areas of the wavelengths' range analysed, these are analogous in behaviour (but reciprocal) to the ensuing chlorophylls' κ_λ, in every biomass sample studied.

Last but not least, the sum of scattering and absorption from all the cell parts and its interaction with the REF in the continuous medium, determines the total optical response of the cell, in the form of attenuation coefficients. In many works, the molecular medium of microalgae cells is adequately characterised as homogeneous having a complex refractive index [4,22,23]. However, if the heterogeneous nature of the cells is considered on the organelle level, the attenuation coefficients might not be reproducible, which is the case on the listed experiences from Fig. (4-a,d). Here a batch culture, with non-nutrient depletion and sufficient light amount has displayed an alteration in the OPs over cultivation time. Even when towards the final moments of the cultivation, biomass concentration started to decrease and, κ_λ and σ_λ decreased as well, it

Table 1
The average value under the PAR spectral range of the coefficients generated by the genetic algorithm employed, corresponding to each sample studied.

	X [g L^{-1}]	0.087	0.130	0.163	0.207	0.248	0.287	0.246	0.159
$\boldsymbol{P}(\mu_{\mathbf{d}}) \geq 0.8$	$(\overline{\mu}_2^*)_{PAR}$	0.9956	0.9946	0.9950	0.9955	0.9935	0.9932	0.9944	0.9941
$0.8 > \boldsymbol{P}(\mu_{\mathbf{d}}) \geq 0.6$	$(\overline{\mu}_3^*)_{PAR}$	0.9874	0.9800	0.9818	0.9842	0.9723	0.9861	0.9795	0.9848
$0.6 > \boldsymbol{P}(\mu_{\mathbf{d}}) \geq 0.4$	$(\overline{\mu}_4^*)_{PAR}$	0.9665	0.9081	0.9451	0.9529	0.9241	0.9685	0.9353	0.9509
$0.4 > \boldsymbol{P}(\mu_{\mathbf{d}}) \geq 0.2$	$(\overline{\mu}_5^*)_{PAR}$	0.7939	0.7696	0.7677	0.8607	0.7918	0.8714	0.7599	0.9247
$0.2 > \boldsymbol{P}(\mu_{\mathbf{d}})$	$(\overline{\mu}_6^*)_{PAR}$	0.6786	0.7300	0.6891	0.5607	0.6145	0.6851	0.6602	0.6732

was not possible to find a linear relationship among these OPs and the biomass quantity (Appendix – Fig. (3-4)). However, in the case of the σ_λ, a lack of linear dependence on the biomass concentration may be explained due to a lack of photoacclimation of the cells. This last highlight the necessity of measuring the radiative properties rapidly and accessibly, to perform correct calculations of the varying light availability inside a PBR.

4.3. The scattering phase function

The primary electromagnetic interaction mechanisms are asserted by the three size regimes: (1) if particles are smaller than the wavelength of light, on which the interaction is mostly determined by scattering and absorption, and the impacting beams' angular distribution is strongly dependent of polarisation. (2) When the particle size almost reaches the wavelengths' size-scale, on which the scattering pattern becomes forward peaking. (3) If the particles' diameter is more massive than the wavelength, on which the interaction is explained through classical-geometrical approaches. The algae' scattering pattern is firmly forward, as many of the more abundant organelles and the cell itself catalogues in between (2) and (3). Roughly 90% of the dispersed light is generally contained within a solid angle of 20 degrees around the optical axis in the forward direction [8].

At the time of calculating the microalgae' OPs, the most general assumptions treat the microorganisms' as well mixed and randomly oriented, on which the cells are presented as symmetric spheroids and, the phenomenon of single scattering prevails due to the consideration of low concentration suspension. Further, the $\beta_{\theta,\lambda}$ is taken as a function dependent on θ angles and finally, as a first-order estimation, $\beta_{\theta,\lambda}$ is assumed to be constant over the PAR spectral region [24]. In this paper, we used a simple physical model of the REF interaction with biological suspensions, relying on the modelling of algae as a continuum where the cells have been replaced with centres of absorption and scattering, randomly distributed throughout the suspension. Later on, a Monte Carlo algorithm can be developed to reproduce the elementary steps of photons flying in the suspension and eventually being removed of it by absorption and scattering events. The likelihood of the latter is linked to the cells' OPs. In our approach, these are provided by a genetic algorithm, making use of Eqs. (12), (13), (14-1), (6) and (15-1), (6).

Based on solid grounds, our proposal here was to reproduce the total light flux and the directional distribution of the beams after travelling throughout a microalgae suspension, constructing 31 independent distribution functions in the wavelengths region $400 < \lambda + 10 < 700\,[nm]$, giving to the MC subroutine the possible forward angles to be selected under the restrictions imposed by Eqs. (12) and (13). In the Table 1, the average in the PAR spectral range of the μ_n^* angles is presented. It can be seen that to simulate the $(Q_\lambda^*)_{EXP}$ values in each sample, up to 80% of the angles taken values of $0^\circ<\theta^\circ<6^\circ$ respect to the optical axis. In a further individual basis, between 80% and 60% of the angles hold values of $9^\circ<\theta^\circ<13^\circ$. The chances for azimuthal angles ranged $15<\theta<24$ is 60% to 40%, while the probabilities of holding $\theta^\circ \leq 40^\circ$ are 40% to 20%. Finally, a likelihood of less than 20% was found for azimuthal angles ranged $43^\circ<\theta^\circ<55^\circ$.

Rather than using $(\mu_n^*)_\lambda$, the values of $(\overline{\mu}_n^*)_{PAR}$ coefficients have been used here mainly for two reasons. In the first place, the variation coefficient of the average of the most probable azimuthal angles is less than 0,3%, while in contrast a 30% of variation can be found in the less probable angles produced. A priori, the latter might lead to think that the 31 sets of $(\mu_n^*)_\lambda$ are wavelength-dependent. However, since the cumulative distribution functions $P(\mu_d)$ were constructed in such a way that the coefficients in the surroundings of $(\mu_d)_\lambda = 1$ hold high chances to be produced, all of the errors associated with the measuring process weight on the less favoured angles to be produced. Therefore, it is expectable to find huge variations among the different $(\mu_n^*)_\lambda$ values. Secondly, rather than elucidate the specific influence of a single element, the nature of these variations is related generally to all of the complex non-absorbing components. So far, the understanding of the individual organelle-light interaction is not sufficiently wide to present a $\beta_{\theta,\lambda}$ function more than partially biased by wavelength [11], like the experiences we have shown in this research.

5. Conclusions

In a purely phototrophic culture, microalgae are dependent on absorbing light energy to meet their demand for cellular functions and growth. This growth is dependent on the light availability inside the reactor, and both quantities are linked through a growth kinetic expression. Addressing the optical properties of a suspension is one of the significant concerns to calculate these kinetics. Cells modify the light field and light modifies the cells. Light exposure and nutrient-level alterations trigger a set of physiological processes in microalgae, on both transcriptional and metabolic levels. These processes affect the OPs of the cells. Therefore, radiation characteristics and the size of the cells are not constant but continually changing as a response to variations in light intensity and colour, among other factors.

In this work, we presented an approach to measure the optical properties of microalgae suspensions. The use of a 3D-printed device in combination with a Monte Carlo approach grant access to how motion and energy carried by photons change throughout culture samples. Utilising an optimisation algorithm/program constrained properly to simulate the light emission in the forward direction, reproducible sets of absorption and scattering coefficients have been calculated, as well as the scattering phase function of the suspension. Further use of the previous information can provide a way of solving the radiative transfer equation for a given system regardless of the assessment of biomass or medium composition.

Declaration of authors' contribution

Manuel Vicente Ibañez: Methodology, Software, Validation, Formal Analysis, Investigation, Writing – Original Draft, Visualisation. **Rodrigo Jorge Leonardi**: Term, Conceptualisation, Methodology, Writing – Review & Editing. **Juliane Steingroewer:** Resources, Supervision, Project administration, Funding acquisition. **Thomas Walther:** Resources, Supervision, Project administration, Funding acquisition. **Heinrich Josué Miguel**: Term, Conceptualisation, Methodology, Writing – Review & Editing. **Krujatz Felix**: Conceptualisation, Investigation, Resources, Writing – Review & Editing, Visualisation, Supervision, Project administration, Funding acquisition.

Statements regarding conflicts, consent, and human/animal rights

No conflicts, informed consent, human or animal rights issues are applicable. The authors declare that there are no conflicts of interest in publishing this article and mutually agree for submission of the manuscript to the Journal of Photochemistry and Photobiology.

Declaration of Competing Interest

The authors declare that they have no known competing for financial interests or personal relationships that could have appeared to influence the work reported in this paper.

Acknowledgements

The research team would like to thank the Deutsch-Argentinisches Hochschulzentrum (DAHZ)/Centro Universitario Argentino-Alemán (CUAA) for their support on joint research projects between German/Argentinian partners.

Supplementary materials

Supplementary material associated with this article can be found, in the online version, at doi:10.1016/j.jpap.2020.100007.

References

[1] J.M. Heinrich, I. Niizawa, F.A. Botta, A.R. Trombert, H.A. Irazoqui, Analysis and design of photobioreactors for microalgae production II: experimental validation of a radiation field simulator based on a Monte Carlo algorithm, Photochem. Photobiol. 88 (2012) 952–960.

[2] C. Posten, C. Walter, Microalgal Biotechnology: Potential and Production, De Gruyter, 2012.

[3] J.M. Heinrich, I. Niizawa, F.A. Botta, A.R. Trombert, H.A. Irazoqui, Analysis and design of photobioreactors for microalgae production I: method and parameters for radiation field simulation, Photochem. Photobiol. 88 (2012) 938–951.

[4] J. Pruvost, J.F. Cornet, F. Le Borgne, V. Goetz, J. Legrand, Theoretical investigation of microalgae culture in the light changing conditions of solar photobioreactor production and comparison with cyanobacteria, Algal Res. 10 (2015) 87–99.

[5] L. Pilon, H. Berberoglu, R. Kandilian, Radiation transfer in photobiological carbon dioxide fixation and fuel production by microalgae, J. Quant. Spectrosc. Radiat. Transf. 112 (2011) 2639–2660.

[6] R. Kandilian, E. Lee, L. Pilon, Radiation and optical properties of *Nannochloropsis oculata* grown under different irradiances and spectra, Bioresour. Technol. 137 (2013) 63–73.

[7] R-L. Heng, L. Pilon, Radiation characteristics and effective optical properties of dumbbell-shaped cyanobacterium Synechocystis sp, J. Quant. Spectrosc. Radiat. Transf. 174 (2016) 65–74.

[8] J. Dauchet, S. Blanco, J.-F. Cornet, R. Fournier, Radiative properties of photosynthetic microorganisms, J. Quant. Spectrosc. Radiat. Transf. 161 (2015) 60–84.

[9] J. Dauchet, S. Blanco, J-F. Cornet, M. El Hafi, V. Eymet, R. Fournier, The practice of recent radiative transfer Monte Carlo advances and its contribution to the field of microorganisms cultivation in photobioreactors, J. Quant. Spectrosc. Radiat. Transf. 128 (2013) 52–59.

[10] E. Lee, R-L. Heng, L. Pilon, Spectral optical properties of selected photosynthetic microalgae producing biofuels, J. Quant. Spectrosc. Radiat. Transf. 114 (2013) 122–135.

[11] R-L. Heng, L. Pilon, Time-dependent radiation characteristics of *Nannochloropsis oculata* during batch culture, J. Quant. Spectrosc. Radiat. Transf. 144 (2014) 154–163.

[12] S. Johnsen, E.A. Widder, The physical basis of transparency in biological tissue: ultrastructure and the minimisation of light scattering, J. Theor. Biol. 199 (1999) 181–198.

[13] R. Kandilian, J. Pruvost, A. Artu, C. Lemasson, J. Legrand, L. Pilon, Comparison of experimentally and theoretically determined radiation characteristics of photosynthetic microorganisms, J. Quant. Spectrosc. Radiat. Transf. 175 (2016) 30–45.

[14] K. Witkowski, T. Krol, A. Zielinski, E. Kuten, A light-scattering matrix for unicellular marine phytoplankton, Limnol. Oceanogr. 43 (1998) 859–869.

[15] R.J. Leonardi, I. Niizawa, H.A. Irazoqui, J.M. Heinrich, Modelling and simulation of the influence of fractions of blue and red light on the growth of the microalga Scenedesmus quadricauda, Biochem. Eng. J. 129 (2018) 16–25.

[16] I. Niizawa, J.M. Heinrich, H.A. Irazoqui, Modelling of the influence of light quality on the growth of microalgae in a laboratory-scale photo-bio-reactor irradiated by arrangements of blue and red LEDs, Biochem. Eng. J. 90 (2014) 214–223.

[17] R.J. Leonardi, M.V. Ibañez, M.N. Morelli, H.A. Irazoqui, J.M. Heinrich, Influence of light stratification on the growth of *Scenedesmus quadricauda*, Biochem. Eng. J. 148 (2019) 97–107.

[18] J-H. Chen, L. Liu, D. Wei, Enhanced production of astaxanthin by *Chromochloris zofingiensis* in a microplate-based culture system under high light irradiation, Bioresour. Technol. 245 (2017) 518–529 Part A.

[19] K.S. Khoo, K. Wayne Chew, G.Y. Yew, W.H. Leong, Y.H. Chaid, P.L. Show, W-H. Chen, Recent advances in downstream processing of microalgae lipid recovery for biofuel production, Bioresour. Technol. 304 (2020) 122996.

[20] Azaman, S. N. A., Nagao, N., Yusoff, F. M., Tan, S. W., Yeap, S. K., 2017. A comparison of the morphological and biochemical characteristics of *Chlorella sorokiniana* and *Chlorella zofingiensis* cultured under photoautotrophic and mixotrophic conditions. doi:10.7717/peerj.3473.

[21] H. Berberoglu, L. Pilon, Experimental measurements of the radiation characteristics of *Anabaena variabilis ATCC 29413-U* and *Rhodobacter sphaeroides ATCC 49419*, Int. J. Hydrog. Energy 32 (2007) 4772–4785.

[22] F. Krujatz, R. Illing, T. Krautwer, J. Liao, K. Helbig, K. Goy, J. Opitz, G. Cuniberti, T. Bley, J. Weber, Light-field-characterization in a continuous hydrogen-producing photobioreactor by optical simulation and computational fluid dynamics, Biotechnol. Bioeng. 12 (2015) 112.

[23] J. Fuente, J. Keller, J.A. Conejero, M. Rögner, S. Rexroth, J.F. Urchueguía, Light distribution and spectral composition within cultures of micro-algae: Quantitative modelling of the light field in photobioreactors, Algal Res. 26 (2017) 166–177.

[24] R. Kandilian, J. Pruvost, J. Legrand, L. Pilon, Influence of light absorption rate by *Nannochloropsis oculata* on triglyceride production during nitrogen starvation, Bioresour. Technol. 163 (2014) 308–319.

[25] Y. Zhang, M. Shi, X. Mao, Y. Kou, J. Liu, Time-resolved carotenoid profiling and transcriptomic analysis reveal mechanism of carotenogenesis for astaxanthin synthesis in the oleaginous green alga *Chromochloris zofingiensis*. Biotechnology for Biofuels, 12- unicellular marine phytoplankton, Limnol. Oceanogr. 43 (2019) 859–869.

[26] Chapter 8Edited by M.N. Özisik, Chapter 8 John Wiley & Sons, New York, 1973, pp. 249–253. Edited by.